Tuning Fluorescence Lifetimes through Changes in Herzberg−Teller Activities: The Case of Triphenylene and Its Hexamethoxy-Substituted Derivative

Eugenio Di Donato, Davide Vanzo, Monica Semeraro, Alberto Credi,* and Fabrizia Negri*

Dipartimento di Chimica 'G. Ciamician', Università di Bologna, Via F. Selmi, 2, 40126 Bologna, Italy, and INSTM, UdR Bologna, Italy

Received: January 18, 2009; Revised Manuscript Received: April 2, 2009

The fluorescence spectra of triphenylene (TP) and 2,3,6,7,10,11-hexamethoxy-triphenylene (HMTP) are measured in glass matrices, and the vibronic structure associated with the electronic spectra is simulated with the help of quantum chemically computed molecular parameters. Franck−Condon (FC) and Herzberg−Teller (HT) mechanisms are included. For excited-state calculations, both configuration interaction with single excitations (CIS) and time-dependent density functional theory (TDDFT) are employed. It is shown that the FC activity is associated with modes of similar shape and frequency in both molecules, while the HT-induced false origins with the largest activity are associated with rather different frequencies and normal coordinates as a result of the mixing and energy lowering of the low-lying allowed excited states in HMTP. The increased HT activity explains the reduced S_1 state lifetime in the substituted TP, in turn driven by the excited-state rearrangement occurring upon substitution of the TP core.

1. Introduction

Triphenylene (TP) is a well-known, high symmetry polycyclic aromatic hydrocarbon (PAH) whose derivatives are largely employed in the fabrication of discotic liquid crystals due to their self-assembly behavior via $\pi\pi$ interactions.[1−4] The very high charge carrier mobility in various mesophases makes these materials suitable for use in one-dimensional conductors,[5,6] solar cells,[7] and light emitting diodes.[8,9] Because of its symmetry, TP is a suitable scaffold for the fabrication of multicomponent assemblies with trigonal symmetry. Recently, a TP derivative was employed in self-assembling host−guest systems[10] and interlocked structures[11] aimed at fabricating molecular machines.[12,13] The promising applications of aggregates of TP derivatives, and other organic molecular materials based on PAH derivatives, depend on molecular properties among which the photophysical properties.

The photophysical properties of TP have been investigated in several studies encompassing fluorescence,[14] absorption,[15] phosphorescence[16] in condensed phases, and more recently laser-induced fluorescence in the gas phase.[17] As for benzene, the electronic transition to and from the lowest excited state of TP is symmetry forbidden and gains intensity through the Herzberg−Teller (HT) mechanism.[18] Theoretical investigations have been reported, based on semiempirical[15,19] and ab initio quantum-chemical calculations,[17,20] also including estimates of HT-induced activities of TP.[17] Photophysical properties of TP derivatives have also been investigated and compared to those of TP,[21] although the differences in the vibronic structure of the fluorescence spectra of TP and TP derivatives have not been analyzed in detail, because of the low resolution of the room temperature spectra.

In this Article, we report the fluorescence spectra and lifetimes of TP and hexa-methoxy triphenylene (HMTP) measured in dichloromethane solution at room temperature and in butyronitrile glass at 77 K (see the Supporting Information for experimental details). A detailed vibronic structure is detected for the first time in the emission spectrum of the hexa-substituted TP derivative at low temperature, which discloses similarities and contrasting features as compared to TP. The experimental spectra are analyzed on the basis of quantum-chemical calculations followed by modeling of spectral activities. More specifically, both HT and FC mechanisms are included in the simulations, and vibronic activities are obtained by computing quantum-chemically all of the relevant molecular parameters (ground- and excited-state atomic structures and vibrational frequencies along with derivatives of transition dipole moments). Radiative lifetimes are also computed, compared to the experimental data, and rationalized in the light of different patterns of electron−phonon couplings in the two molecules.

2. Quantum Chemical Calculations

The ground-state structure and harmonic vibrational frequencies of the two chromophores were investigated at the ab initio HF level and using density functional theory (DFT) with the B3LYP hybrid functional. Vertical electronic excitation energies were obtained with time-dependent (TD)DFT and configuration interaction singles (CIS) methods. Although the latter is known to overestimate excitation energies, it provides a reasonable description for excited states dominated by single excitations. Excited-state geometries and vibrational frequencies were determined with the CIS and TDDFT methods. The split-valence 6-31G* basis set was employed for HF, CIS, and single-point TDDFT calculations. The def-SVP basis set[22] was employed for ground- and excited-state geometry optimization and harmonic vibrational frequency calculations carried out at DFT and TDDFT levels. HF, CIS, and single-point TDDFT calculations were carried out with the Gaussian 03[23] suite of programs. Although it is known that the TDDFT is generally superior to the CIS approach,[24,25] analytical gradients are not available in Gaussian 03,[23] and for this reason geometry optimization of the ground and excited states with DFT and TDDFT methods, respectively, was carried out with the TURBOMOLE 5.9 program package.[26,27] Because a systematic comparison between

* Corresponding author. E-mail: fabrizia.negri@unibo.it (F.N.); alberto.credi@unibo.it (A.C.).

10.1021/jp9005247 CCC: $40.75
Published on Web 05/19/2009

the two methods (CIS and TDDFT) as regards the prediction of FC and HT spectroscopic parameters has not been reported extensively, we believe it can be of interest to compare the performance of the two methods.

3. Franck−Condon and Herzberg−Teller Contributions to Vibronic Activity

Within the Born−Oppenheimer approximation, the transition dipole moment between vibronic states, that is, vibrational states m and n belonging to two electronic states K and J, is

$$M_{Km,Jn} = \langle K, m|\mu|J, n\rangle = \langle m|\mu_{K,J}|n\rangle \quad (1)$$

where $\mu_{K,J}$ is the electronic transition dipole moment, and m and n are multidimensional vibrational wave functions. According to the HT mechanism, we can expand the transition dipole moment as a Taylor series in the nuclear coordinates about the equilibrium nuclear configuration

$$M_{Km,Jn} = \mu^{o}_{K,J}\langle m|n\rangle + \sum_i \left(\frac{\partial \mu_{K,J}}{\partial Q_i}\right)\langle m|Q_i|n\rangle + \ldots \quad (2)$$

When the electronic transition dipole moment $\mu^{o}_{K,J}$ vanishes for symmetry reasons, as is the case for TP and HMTP, the second term in eq 2 accounts for the vibronic structure observed in the electronic spectra. Each $((\partial\mu_{K,J})/(\partial Q_i))$ first derivative with respect to non totally symmetric (NTS) modes may contribute intensity to the HT induced false origins in the spectra[28] from which progressions of FC active totally symmetric (TS) modes originate. Assuming the harmonic approximation, negligible normal mode rotation (Duschinsky effect) upon excitation, and identical frequencies in the K and J electronic states, the intensity of each false origin (0→1 for the ith NTS mode) in the spectrum, when all other vibrational wave functions are in their ground state, is given by

$$\begin{aligned} I_{K0_i^{NTS},J1_i^{NTS}} &\propto M^2_{K0_i^{NTS},J1_i^{NTS}} \\ &= \left[\left(\frac{\partial \mu_{K,J}}{\partial Q_i}\right)\langle 0_i|Q_i|1_i\rangle\right]^2 \\ &= \left[\left(\frac{\partial \mu_{K,J}}{\partial Q_i}\right)\sqrt{\frac{\hbar}{m\omega_i}}\langle 0_i|q_i|1_i\rangle\right]^2 \\ &= \left[\left(\frac{\partial \mu_{K,J}}{\partial Q_i}\right)\sqrt{\frac{\hbar}{2m\omega_i}}\right]^2 \end{aligned} \quad (3)$$

where the vibrational integral is expressed in dimensionless coordinates q_i, with $\langle 0_i|q_i|1_i\rangle = (1/2)^{1/2}\langle 1_i|1_i\rangle$.

The derivatives in eq 3 were evaluated numerically by displacing the molecular geometry along NTS normal coordinates and using both CIS and TDDFT levels of theory to evaluate electronic transition dipole moments. Two displacements, obtained by multiplying the Cartesian normal coordinates by 0.02 and 0.1, were considered and gave negligible differences in the computed induced transition dipole moments. Excited-state normal coordinates and frequencies were employed to estimate induced intensities in absorption spectra, while ground-state normal coordinates and frequencies were employed to estimate intensities of false origins in the emission spectra. For each computed transition dipole moment, the associated oscillator strength contribution can be obtained as

$$f_i = \frac{2}{3}h\nu_{K0_i^{NTS},J1_i^{NTS}}M^2_{K0_i^{NTS},J1_i^{NTS}} \quad (4)$$

where $h\nu_{K0_i^{NTS},J1_i^{NTS}}$ is the energy difference between the selected vibronic states of the K↔J electronic transition in hartree, whose 0−0 energy was taken from the experimental data (see below), and M is in e·bohr.

Finally, the radiative lifetime was determined from the common work form[29] of the Strickler−Berg equation[30] by summing over the oscillator strengths computed for all of the false origins:

$$\tau = \frac{1.497}{n^2\langle\nu\rangle^2\sum_{i=1}^{NTS} f_i} \quad (5)$$

where $\langle\nu\rangle$ is the average energy associated with the transition (usually assumed to be equal to the 0−0 energy) in wavenumbers, and n is the refraction index. We calculated the radiative times either by using the simple 0−0 energy approximation or by computing the average energy $\langle\nu\rangle = \sum_{i=1}^{NTS}(\nu_{K0_i^{NTS},J1_i^{NTS}}p_i)$ by summing over all of the vibronic energies associated with false origins in the spectra, multiplied by a weighting factor p_i given by $p_i = (f_i)/(\sum_{j=1}^{NTS}(f_j))$. As it will be shown, the resulting radiative lifetimes are only slightly different from those obtained by using simply the 0−0 energy.

The FC structure[31−35] associated with each false origin in both absorption and emission spectra was evaluated along the lines described in previous work.[20] Assuming the harmonic approximation, negligible Duschinsky effect, and identical frequencies in the K and J states, we obtained for each ith totally symmetric mode the displacement parameters B_i relative to the S_0↔S_n transition. The latter are defined as

$$B_i = \sqrt{\frac{\omega_i}{\hbar}}\{X_K - X_J\}\mathbf{M}^{1/2}L_i(K) \quad (6)$$

where X_K is the $3N$ dimensional vector of the equilibrium Cartesian coordinates of the Kth state (here S_0 or S_1), $\mathbf{M}$ is the $3N \times 3N$ diagonal matrix of the atomic masses, and $L_i(K)$ is the $3N$ vector describing the normal coordinate Q_i of the K state in terms of mass-weighted Cartesian coordinates. In the harmonic approximation and assuming identical frequencies in the two electronic states, the intensity of a band corresponding to the $n = [n_1,n_2,n_3,\ldots n_{TS}]$ vibrational quantum (TS modes) and originating from the false origin induced by the ith NTS mode is given by

$$I_{K0_i^{NTS}0^{TS},J1_i^{NTS}n^{TS}} \propto \left[\left(\frac{\partial \mu_{K,J}}{\partial Q_i}\right)\sqrt{\frac{\hbar}{2m\omega_i}}\right]^2\prod_j^{TS} e^{-\gamma_j}\frac{(\gamma_j)^{n_j}}{n_j!} \quad (7)$$

where $\gamma_i = (1/2)(B_i)^2$.

To account for the Duschinsky[36] normal mode mixing, vibrations of the ground state were considered in the simulation of the emission spectra, and vibrational modes of the excited state were considered in the simulation of the absorption spectra.[37] While this approach is approximate, and less rigorous than that discussed in recent work,[24,25,31−35,38,39] it is justified

by the minor Duschinsky rotation upon excitation, computed for the active frequencies.

Two combinations of computed parameters (hereafter indicated as Set1 and Set2) were considered: in one simulation (Set1), HF (S_0) and CIS (S_1) geometries were considered, and normal modes and frequencies of the ground state (HF level, frequencies scaled by 0.9) or excited state (CIS level, frequencies scaled by 0.9) were employed in the calculation of FC and HT activities. In the second simulation (Set2), B3LYP (S_0) and TDDFT (S_1) geometries and normal coordinates were used to estimate FC and HT intensities, and vibrational frequencies were not scaled. The normal mode mixing upon excitation was evaluated by computing the Duschinsky normal coordinate rotation matrices.[36] These were employed also to correlate normal coordinates (and vibrational frequencies) calculated at different levels of theory for the same molecule. In addition, mode mixing and correlation between the ground-state (HF/6-31G*) normal coordinates and frequencies of TP and HMTP were also evaluated by calculating the appropriate Duschinsky matrix.

Finally, the simulated spectra were built using the experimentally determined 0−0 energy (29 618 cm^{-1} from the gas-phase TP spectrum,[17] 29 287 cm^{-1} from the TP emission spectrum in BN, 27 905 cm^{-1} from the emission spectrum of HMTP in BN) and by superimposing each computed spectral line with a Lorentzian line width of 3 cm^{-1} for high-resolution spectra and of 150 cm^{-1} for comparison with the spectra measured in the condensed phase.

4. Results and Discussion

4.1. Ground- and Excited-State Structures. The ground-state (D_{3h} symmetry) equilibrium structure of TP computed in this work agrees with the results of previous studies.[40] For HMTP, the symmetry point group is also D_{3h}, although there are several possible conformers of lower symmetry determined by different orientations of the six alkoxyl substituents. We chose to run the calculations for the high symmetry structure, for which the S_0−S_1 electronic transition is symmetry forbidden as for TP, even because the computed energy (B3LYP/6-31G*) of the lower symmetry conformers is considerably higher (ca. 4−5 kcal/mol) than that of the higher symmetry structure. The presence of lower symmetry conformers, however, may account for the 0−0 band observed for HMTP (in this work) and in general for 2,3,6,7,10,11-substituted derivatives of TP,[21] although, due to symmetry breaking in condensed phases, the fluorescence spectra of TP and TP derivatives can show traces of otherwise forbidden spectral origins[14] even in the absence of lower symmetry conformers. A graphical representation of selected optimized bond lengths of the ground state of TP and HMTP is shown in Figures S1 and S2 of the Supporting Information. The CC bond numbering adopted is defined in Figure 1 where the structures of TP and HMTP are shown. The results of HF/6-31G* and B3LYP/def-SVP are similar, although the bond length alternation is predicted to be more remarkable, as expected, at the HF level, especially for the central benzene ring. The equilibrium structure of the lowest singlet excited state of TP (the A_1' state) was determined in previous studies with semiempirical methods.[15] Here, we employed the CIS/6-31G* and TDDFT/def-SVP* levels of theory to determine the equilibrium structure along with vibrational frequencies and normal modes. A graphical representation of selected optimized bond lengths of the lowest excited state of TP and HMTP is shown in Figures S3 and S4. While TDDFT correctly predicts the A_1' state as the lowest singlet excited state, CIS calculations

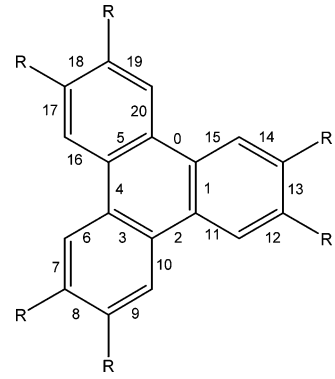

Figure 1. Structural formula and bond numbering adopted for TP and HMTP. R = H for TP; R = OCH_3 for HMTP.

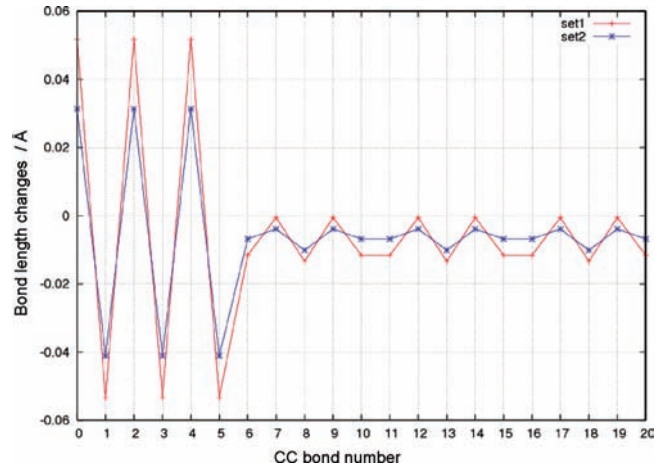

Figure 2. Comparison between CC bond length changes upon $S_0 \rightarrow S_1$ excitation of TP, computed for Set1 (red) and Set2 (blue). CC bond numbering is defined in Figure 1.

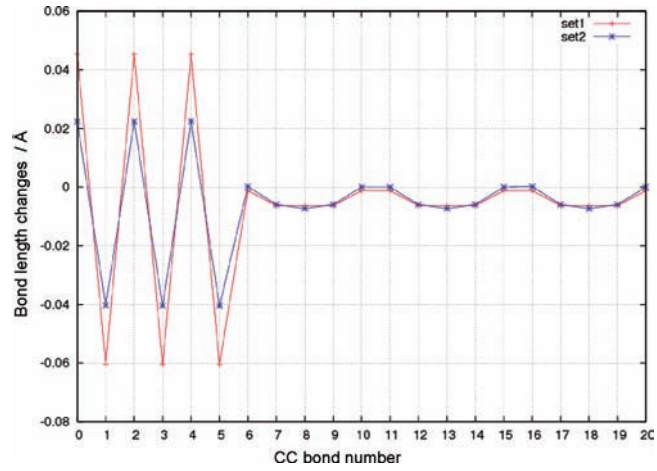

Figure 3. Comparison between CC bond length changes upon $S_0 \rightarrow S_1$ excitation of HMTP, computed for Set1 (red) and Set2 (blue). CC bond numbering is defined in Figure 1.

predict an inversion between the two lowest excited states of TP and HMTP, in contrast with the experimental evidence. In agreement with its correct assignment, in the following we will use the label S_1 for the A_1' state irrespective of the level of theory employed to determine it. Computed and observed $S_0 \leftrightarrow S_1$ excitation energies of TP and HMTP are collected in Table S1. It is interesting to compare the geometry change upon $S_0 \rightarrow S_1$ excitation predicted by HF/CIS (Set1) and DFT/TDDFT (Set2) calculations for the two molecules, because this parameter is relevant for the simulation of FC activities. Selected CC bond

TABLE 1: Computed FC Parameters (γ Parameters in Eq 7) for the TS Modes of TP and HMTP[a]

Set1				Set2			
HF frequency[b] cm^{-1}	γ^c ($S_1 \rightarrow S_0$)	CIS frequency[b] cm^{-1}	γ^c ($S_0 \rightarrow S_1$)	B3LYP frequency[d] cm^{-1}	γ^e ($S_1 \rightarrow S_0$)	TDDFT frequency[d] cm^{-1}	γ^e ($S_0 \rightarrow S_1$)
				TP			
401	0.00	408	0.00	423	0.05	425	0.06
686(693)[f]	0.09	**653**(657)[f]	0.12	**712**(693)[f]	0.11	**686**	0.12
1019	0.06	1032	0.02	1090	0.05	1068	0.03
1113	0.01	**1278**	0.18	1259	0.10	1310	0.03
1190	0.00	1158	0.07	1196	0.01	1184	0.01
1296(1336)[f]	0.45	1421(1444)[f]	0.00	**1385**(1336)[f]	0.35	**1401**(1371)[f]	0.46
1466(1456)[f]	0.26	**1345**(1371)[f]	0.39	**1487**(1456)[f]	0.19	**1509**(1444)[f]	0.13
1562	0.01	1527	0.01	1595	0.01	1536	0.01
				HMTP			
164	0.02	164	0.02	168	0.05	172	0.06
284		286		297	0.07	298	0.07
400		402		418		420	
711	0.09	**685**	0.12	**738**	0.12	**719**	0.13
832		833		864		859	
1076		1082		1109		1104	
1127	0.01	1312	0.04	1255	0.04	1290	0.03
1207		1202		1213		1213	
1275	0.20	**1281**	0.16	1320		1363	0.04
1383	0.44	**1369**	0.40	**1429**	0.41	**1430**	0.35
1471	0.02	1475	0.02	1472	0.03	1478	0.02
1496	0.01	1496		1483	0.01	1481	0.02
1501	0.07	1440	0.06	1534		1510	0.02
1558	0.01	1553		1594	0.02	1594	

[a] The correlation between frequencies computed at different levels of theory is based on inspection of the Dushinsky mode mixing matrices. CH stretching frequencies are excluded. Frequencies displaying the largest FC activities are in bold. [b] 6-31G* basis set, frequency scaled by 0.9. [c] Computed from HF ground-state geometry and CIS excited-state geometry, scaled by 0.5. [d] def-SVP basis set, unscaled frequency. [e] Computed from B3LYP ground-state geometry and TDDFT excited-state geometry, unscaled. [f] Exp value from ref 17.

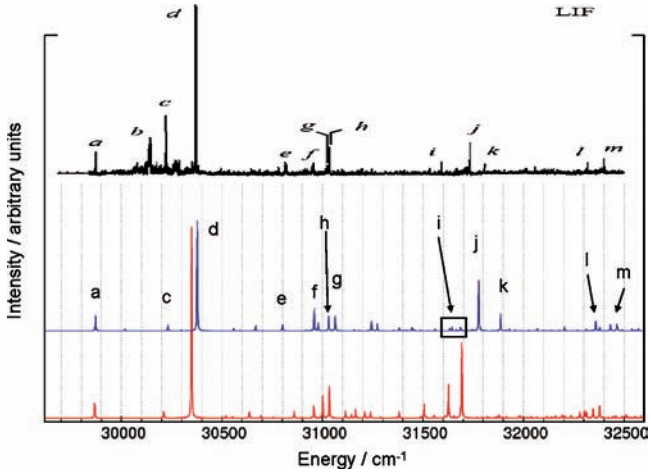

Figure 4. Comparison between the experimental LIF spectrum in the gas phase (top, black) and the simulated absorption spectra from Set1 (red) and Set2 (blue).

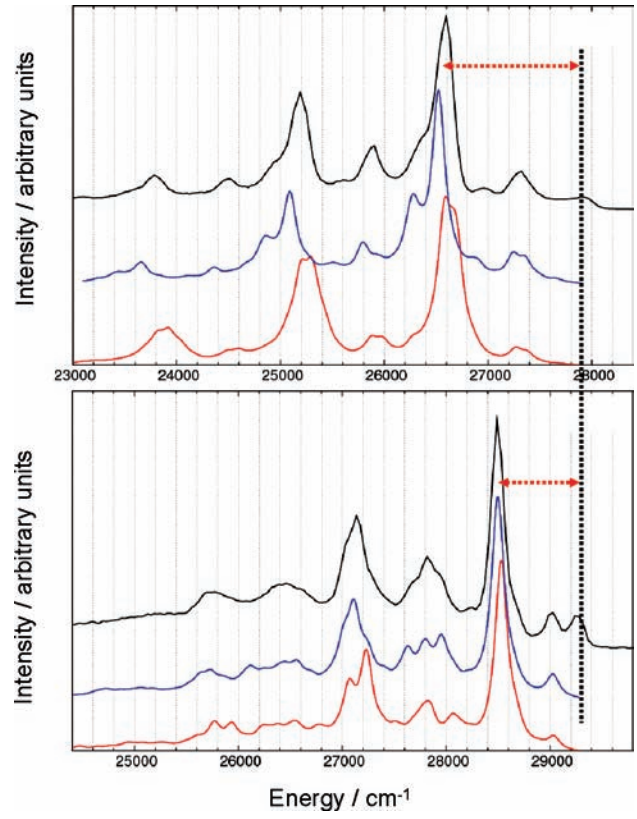

Figure 5. Comparison between the experimental (black) fluorescence spectra of TP (bottom panel) and HMTP (top panel) in butyronitrile glass at 77 K and the simulated emission spectra from Set1 (red) and Set2 (blue) computed parameters.

length changes upon excitation are represented in Figure 2 for TP and Figure 3 for HMTP. The figure shows that the geometry change is predicted to be similar for the two sets, but the magnitude of CC bond changes is considerably smaller for Set2 (DFT/TDDFT level). This fact is reflected in the magnitude of the FC activity parameters (γ parameters in eq 7) computed for Set1 and Set2 and in the simulated vibronic structure as discussed below. For a given level of theory (Set1 or Set2), the geometry change is similar for TP and HMTP, as expected given the similar nature of the lowest excited state for the two molecules.

4.2. Electronic Spectra and Photophysics. The computed FC parameters are collected in Table 1 for TP and HMTP, respectively. Both molecules show the largest activities (that is the largest γ parameters) for very similar frequencies (indicated in bold in Table 1) and vibrational normal modes, as seen in more detail in Figure S5 of the Supporting Information, where

TABLE 2: Computed HT Activities for the NTS Modes (e′ Symmetry) of TP[a]

Set1				Set2					
HF frequency[b] cm^{-1}	$M^2_{\tilde{S}_1 0, S_0 1}$[c] $(e\cdot bohr)^2 \times 10^4$	CIS frequency[b] cm^{-1}	$M^2_{\tilde{S}_0 0, S_1 1}$[c] $(e\cdot bohr)^2 \times 10^4$	B3LYP frequency[d] cm^{-1}	$M^2_{\tilde{S}_1 0, S_0 1}$[e] $(e\cdot bohr)^2 \times 10^4$	TDDFT frequency[d] cm^{-1}	$M^2_{\tilde{S}_0 0, S_1 1}$[e] $(e\cdot bohr)^2 \times 10^4$	exp emission	exp absorption
251	20	249	20	260	20	255	22	283,[f]259[g]	247,[f]258[h]
392	4	388		410		401	2	406[g]	368[h]
612	28	594	8	635	9	614	6	620,[f]623[g]	597,[f]598[h]
757	299	**731**	268	**790**	170	**760**	161	770,[f]769[g]	745[f,h]
978		935	2	1021		973	2		
1044	12	1019	8	1077	6	1051	6	1048[g]	
1096	2	1078	2	1134		1109			
1142	12	1150		1179	1	1153			
1208	19	1241	6	1332	36	1341	31	1299[g]	1332,[f]1330[h]
1238	18	1230		1266	5	1235			
1319	2	1341	18	1382	2	1362	8		
1439	20	1417	44	1467	13	1413	21		1414[f]
1508	25	1497	6	1535	4	1510			
1603	16	1548	10	1631		1540	2		
1637	2	1622	6	1664	23	1627	15		

[a] The correlation between frequencies computed at different levels of theory is based on inspection of the Dushinsky mode mixing matrices. CH stretching frequencies are excluded. Frequencies displaying the largest HT activities are in bold. [b] 6-31G* basis set, frequency scaled by 0.9. [c] Transition dipole moment derivatives in eq 3 computed from CIS/6-31G* calculations. [d] def-SVP basis set, unscaled frequency. [e] Transition dipole moment derivatives in eq 3 computed from TDDFT B3LYP/6-31G* calculations. [f] Exp value from ref 17. [g] Exp value from ref 14. [h] Exp value from ref 15.

the TS normal modes of TP are shown and correlated with those of HMTP. It is worth noting (see Table 1) that the FC parameters predicted by HF/CIS calculations (Set1) are considerably larger[24] than those predicted at DFT/TDDFT level (Set2) and a remarkable, although uniform, scaling factor (0.5) had to be introduced to obtain the values listed in Table 1. The scaled values agree with the results of Set2 (unscaled) and, more important, with the activities shown in the experimental spectra.

The computed HT activities of e′ modes are collected in Table 2 for the emission and absorption spectra of TP and in Table 3 for the emission spectra of HMTP. In the two tables, the frequencies displaying the largest HT activity are indicated in bold. In contrast with the FC activity, the HT activity is not comparable for the two molecules. The most striking difference is that for TP the largest activity is computed for e′ modes of ca. 750 cm^{-1}, while frequencies above 1200 cm^{-1} contribute most of the HT activity of HMTP. A more thorough inspection of Table 3 shows indeed some HT intensity computed for HMTP around 650 cm^{-1}, for vibrational modes that correlate with those active in TP (see Figure S6 in the Supporting Information, where the e′ normal modes of TP are shown and correlated with those of HMTP via inspection of Duschinsky mode mixing matrices). Interestingly, the normal modes of HMTP displaying the largest HT activity (frequencies above 1200 cm^{-1}) also have a counterpart in TP (see Figure S6), although the corresponding TP modes are practically inactive.

The data collected in Tables 1−3 were employed to simulate the $S_0 \leftrightarrow S_1$ absorption and emission spectra of TP and the emission spectrum of HMTP. The two simulated high-resolution absorption spectra (from Set1 and Set2 computed parameters) of TP are compared to the LIF spectrum observed in the gas phase[17] in Figure 4. The quality of both simulated spectra is very satisfactory, with the spectrum corresponding to Set2 showing a remarkable agreement with the observed fine structure, mostly because of a better prediction of excited-state frequencies. The Set2 spectrum is similar to a previously reported simulation,[17] but it incorporates also the intensities of all TS progressions (based on quantum-chemically computed γ parameters) associated with the computed false origins. As a consequence, some additional bands appear in the simulated spectrum, resulting in a slightly different assignment for some of the observed bands. A detailed analysis of the simulated bands and their correlation with bands observed in the LIF gas-phase

TABLE 3: Computed HT Activities for the NTS Modes (e′ Symmetry) of HMTP[a]

Set1		Set2	
HF frequency[b] cm^{-1}	$M^2_{\tilde{S}_1 0, S_0 1}$[c] $(e\cdot bohr)^2 \times 10^4$	B3LYP frequency[d] cm^{-1}	$M^2_{\tilde{S}_1 0, S_0 1}$[e] $(e\cdot bohr)^2 \times 10^4$
100	2	104	2
174	2	179	
238	12	245	14
357		371	2
408	14	423	14
527	126	**548**	76
617	18	641	2
642	164	**666**	92
774		802	
971	12	1008	40
1050	122	1081	28
1083	2	1102	
1164		1192	
1194	537	1231	2
1199	249	1207	22
1217	292	1314	1
1238	625	1250	2
1319	865	**1327**	88
1332	927	**1381**[f]	666
1427	103	1453	11
1466	2	1466	2
1478	34	1501	5
1495	12	1479	7
1496		1481	4
1535	54	1567	12
1611	90	**1629**	217
1648	101	1668	4

[a] The correlation between frequencies computed at different levels of theory is based on inspection of the Dushinsky mode mixing matrices. CH stretching frequencies are excluded. Frequencies displaying the largest HT activities are in bold. [b] 6-31G* basis set, frequency scaled by 0.9. [c] Transition dipole moment derivatives in eq 3 computed from CIS/6-31G* calculations. [d] def-SVP basis set, unscaled frequency. [e] Transition dipole moment derivatives in eq 3 computed from TDDFT B3LYP/6-31G* calculations. [f] Inspection of the Duschinsky matrix (see Table S4 in the Supporting Information) shows a strong mode mixing between B3LYP and HF computed frequencies in this region, partly responsible for the different HT intensity distribution computed at the two levels of theory.

spectrum[17] and in the condensed phase absorption spectrum[15] is summarized in Table S2. The inclusion of FC progressions in the simulated spectra is of particular relevance for the comparison (see Figure 5) with the low temperature fluorescence spectra of TP and HMTP measured in butyronitrile at 77 K, showing an extended vibronic structure. The spectra of the two molecules are intentionally aligned along the weak 0−0 band, as indicated by the vertical black dotted line crossing the two spectra in Figure 5, to facilitate the identification of similar and contrasting features in the spectra. The two spectra show an overall similar vibronic extension, due to similar FC activities, nicely reproduced by the calculations. However, as indicated by the red dotted arrows in the figure, the most prominent band in the spectra is shifted, with respect to the 0−0 band, by remarkably different frequencies. This major spectral feature is correctly reproduced by both sets of simulated spectra (FC parameters for Set1 had to be scaled as discussed above) and rationalized in terms of different HT activities in the two molecules. A detailed assignment of the most prominent bands in the fluorescence of HMTP is summarized in Table S3.

Another important photophysical parameter is the fluorescence lifetime, which was determined in earlier investigations for TP as well as for many of its derivatives. Specifically, the lifetime of TP was found to be on the order of 36−38 ns at room temperature in a variety of deoxygenated organic solvents[41,42] and 41 ns in the gas phase.[17] In this work, we measured the fluorescence lifetimes of TP and HMTP in air equilibrated CH_2Cl_2 at room temperature and in butyronitrile glass at 77 K. For TP, we found a lifetime $\tau_F = 9.5$ ns at room temperature and 46 ns at low T, whereas for HMTP we determined $\tau_F = 8.7$ ns at room temperature and 34 ns at low T, in good agreement with the fluorescence lifetime reported for similar TP derivatives.[21] We also determined the fluorescence quantum yield (Φ_F) values in air equilibrated CH_2Cl_2, which resulted to be 0.028 for TP and 0.089 for HMTP. We then computed the radiative lifetimes according to eq 5, setting the refraction index to 1.42 and approximating $\langle\nu\rangle$ to the 0−0 energy, and found 337 ns (204 ns) for TP and 88 ns (27 ns) for HMTP from Set2 (Set1) calculations, respectively. Using a more appropriate average energy for $\langle\nu\rangle$, we get 362 ns (218 ns) for TP and 97 ns (29 ns) for HMTP from Set2 (Set1) calculations, respectively. The computed radiative lifetimes depend on the level of theory and are expected to be longer than the observed fluorescence lifetime values, due to the neglect of nonradiative processes in their evaluation. The computed values τ_{rad}^{calc} can be compared to the experimental radiative lifetimes $\tau_{rad}^{exp} = \tau_F/\Phi_F$ obtained from the observed fluorescence lifetimes and fluorescence quantum yields. These result to be 339 ns for TP and 97 ns for HMTP, in excellent agreement with the computed values (Set2) discussed above. Furthermore, the role of the value assumed for $\langle\nu\rangle$ in eq 5 is minor because the energy extension of the fluorescence spectrum is minor as compared to the magnitude of the 0−0 energy. On the basis of the results of the calculations, it can be concluded that the different HT activities of the two molecules is the dominant factor influencing, in turn, their radiative lifetimes.

With the purpose of deepening our understanding on the different HT activity of HMTP, we have examined the lowest excited states of TP and its derivative. The 50 lowest excited states were evaluated for both molecular systems with CIS and TDDFT calculations and employed to plot the $S_0 \rightarrow S_n$ absorption spectra shown in Figure 6 (TDDFT results) and in Figure S7 (CIS results, see the Supporting Information). The TDDFT computed spectra predict a bathochromic shift of the first strong band in the absorption spectrum of HMTP as compared to TP, in excellent agreement with the observed data. Calculations indicate that there are at least two E′ states contributing to the first strong experimental band, the lowest of which shows a larger transition dipole moment than the second, in the case of HMTP. Inspection of the wave function of these two states shows that moving from TP to HMTP, the orbitals involved in electronic excitation change little (Figure S8, Supporting Information), but the two states mix and move to lower energies, with the first of the two lowering more than the second. As a result, for HMTP, the intensity induced through the HT mechanism will be enhanced for those modes coupled more strongly to the lowest of the two E′ states, due to the reduced energy gap between the coupled states and to a moderately different nature of the E′ excited states. The strongly active modes of HMTP (with frequencies above 1200 cm^{-1}) are likely to be activated by such mechanism, as implied by the results of additional TDDFT calculations of HT-induced activities carried out with reduced orbital spaces, shown in more detail in Figure S9 in the Supporting Information. A similar change in excited states is computed from CIS calculations (Figure S7) with a slightly stronger mixing of the E′ excited states of HMTP, accounting for the comparably larger HT activity of modes above 1200 cm^{-1} computed from Set1 as shown in Table 3. Both sets of calculations concur to the same conclusion, that a mixing occurs among the lowest allowed excited states of E′ symmetry when moving from TP to HMTP, thereby enhancing the activity of e′ modes of higher frequency for HMTP.

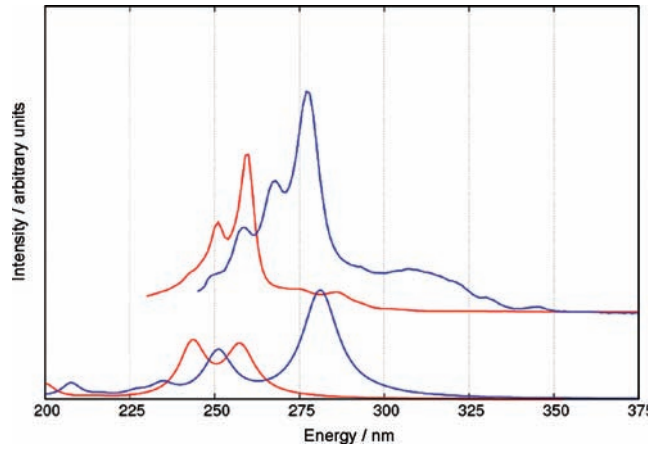

Figure 6. Comparison between TDDFT computed (bottom) $S_0 \rightarrow S_n$ absorption spectra of TP (red) and HMTP (blue) and their respective observed absorption spectra measured in CH_2Cl_2 solution at room temperature (top). The computed spectra show a reduced structure because the vibronic structure associated with electronic transitions was not included.

5. Concluding Remarks

We have recorded the absorption spectra, the fluorescence spectra, and lifetimes of TP and HMTP at room temperature and 77 K. To assist the interpretation of the vibronic structure observed in the experimental spectra and to rationalize the different photophysical properties of the TP derivative, FC and HT contributions to the vibronic activity in the electronic spectra of TP and HMTP have been evaluated on the basis of quantum-chemically computed molecular parameters. Duschinsky mode mixing matrices are computed to correlate ground state with excited-state normal modes and also TP vibrational modes and frequencies with those of HMTP.

The calculations show that the FC activity in the spectra of the two parent molecules is governed by similar vibrational

frequencies, associated with similar nuclear motions, for TP and HMTP. In contrast, the most active HT modes are remarkably different (in frequency and shape) for the two molecules. The similar FC structure in the spectra derives from the similar nature of the lowest singlet excited state. The contrasting distribution of HT-induced vibronic intensities in TP and HMTP is shown to be driven by a mixing and concomitant energy lowering of low-lying symmetry-allowed excited states from which intensity is stolen through the HT mechanism. This mechanism is in turn responsible for the reduced lifetime of the lowest excited state of HMTP. Although this study confirms that TDDFT (Set2) is superior[24,25,32,33,38] to CIS (Set1) and provides a more quantitative agreement, it is interesting to note that both sets of computed parameters employed in this work concur to the same interpretation of the observed phenomenon and provide simulated spectra of similar quality once the FC parameters computed for Set1 are scaled.

In summary, TP and HMTP represent an example of how the photophysical properties of a PAH may be tuned by chemical substitution, thereby modulating the electronic structure and electron−phonon coupling patterns. The study suggests a link between chemical substitution, modulation of electronic structure, and electron−phonon couplings and resulting photophysical properties that may be of use in the design of optimized PAHs for the fabrication of self-assembled columnar phases[43] and for the design of supramolecular systems.[12]

Acknowledgment. This work was supported by funds from MIUR (PRIN 2006034123 and grant 60%) and Regione Emilia-Romagna (Net-lab PROMINER). We are indebted with the referees for their comments and suggestions that contributed to improve the manuscript.

Supporting Information Available: Materials and methods, four tables including computed and observed excitation energies, detailed assignments of the absorption spectra of TP, fluorescence spectra of HMTP, Duschinsky mode mixing matrix for HMTP, and nine figures including equilibrium structure data, correlation between normal modes of TP and HMTP, CIS computed $S_0 \rightarrow S_n$ absorption spectra, TP and HMTP frontier orbitals, and modulation of HT activities with TDDFT calculations in restricted orbital spaces. This material is available free of charge via the Internet at http://pubs.acs.org.

References and Notes

(1) McKenna, M. D.; Barbera, J.; Marcos, M.; Serrano, J. L. *J. Am. Chem. Soc.* **2005**, *127*, 619–625.
(2) Ikeda, M.; Takeuchi, M.; Shinkai, S. *Chem. Commun.* **2003**, 1354–1355.
(3) Barbera, J.; Garces, A. C.; Jayaraman, N.; Omenat, A.; Serrano, J. L.; Stoddart, J. F. *Adv. Mater.* **2001**, *13*, 175–180.
(4) Paraschiv, I.; Giesbers, M.; van Lagen, B.; Grozema, F. C.; Abellon, R. D.; Siebbeles, L. D. A.; Marcelis, A. T. M.; Zuilhof, H.; Sudholter, E. J. R. *Chem. Mater.* **2006**, *18*, 968–974.
(5) Adam, D.; Closs, F.; Frey, T.; Funhoff, D.; Haarer, D.; Ringsdorf, H.; Schuhmacher, P.; Siemensmeyer, K. *Phys. Rev. Lett.* **1993**, *70*, 457–460.
(6) Adam, D.; Schuhmacher, P.; Simmerer, J.; Haussling, L.; Siemensmeyer, K.; Etzbach, K. H.; Ringsdorf, H.; Haarer, D. *Nature* **1994**, *371*, 141–143.
(7) Oukachmih, M.; Destruel, P.; Seguy, I.; Ablart, G.; Jolinat, P.; Archambeau, S.; Mabiala, M.; Fouet, S.; Bock, H. *Sol. Energy Mater. Sol. Cells* **2005**, *85*, 535–543.
(8) Freudenmann, R.; Behnisch, B.; Hanack, M. *J. Mater. Chem.* **2001**, *11*, 1618–1624.
(9) Seguy, I.; Jolinat, P.; Destruel, P.; Farenc, J.; Mamy, R.; Bock, H.; Ip, J.; Nguyen, T. P. *J. Appl. Phys.* **2001**, *89*, 5442–5448.
(10) Balzani, V.; Clemente-Leon, M.; Credi, A.; Lowe, J. N.; Badjic, J. D.; Stoddart, J. F.; Williams, D. J. *Chem.-Eur. J.* **2003**, *9*, 5348–5360.
(11) Badjic, J. D.; Balzani, V.; Credi, A.; Lowe, J. N.; Silvi, S.; Stoddart, J. F. *Chem.-Eur. J.* **2004**, *10*, 1926–1935.
(12) Badjic, J. D.; Balzani, V.; Credi, A.; Silvi, S.; Stoddart, J. F. *Science* **2004**, *303*, 1845–1849.
(13) Badjic, J. D.; Ronconi, C. M.; Stoddart, J. F.; Balzani, V.; Silvi, S.; Credi, A. *J. Am. Chem. Soc.* **2006**, *128*, 1489–1499.
(14) Lamotte, M.; Risemberg, S.; Merle, A.-M.; JoussotDubien, J. *J. Chem. Phys.* **1978**, *69*, 3639–3646.
(15) Chojnacki, H.; Laskowski, Z.; Lewanowicz, A.; Ruziewicz, Z.; Wandas, R. *Chem. Phys. Lett.* **1986**, *124*, 478–482.
(16) Nishi, N.; Matsui, K.; Kinoshita, M.; Higuchi, J. *Mol. Phys.* **1979**, *38*, 1–24.
(17) Kokkin, D. L.; Reilly, N. J.; Troy, T. P.; Nauta, K.; Schmidt, T. W. *J. Chem. Phys.* **2007**, *126*, 084304.
(18) Herzberg, G.; Teller, E. *Z. Phys. Chem. B* **1933**, *21*, 410.
(19) Baunsgaard, D.; Harrit, N.; El Balsami, M.; Negri, F.; Orlandi, G.; Frederiksen, J.; Wilbrandt, R. *J. Phys. Chem. A* **1998**, *102*, 10007–10016.
(20) Keszthelyi, T.; Balakrishnan, G.; Wilbrandt, R.; Yee, W. A.; Negri, F. *J. Phys. Chem. A* **2000**, *104*, 9121–9129.
(21) Baunsgaard, D.; Larsen, M.; Harrit, N.; Frederiksen, J.; Wilbrandt, R.; Stapelfeldt, H. *J. Chem. Soc., Faraday Trans.* **1997**, *93*, 1893–1901.
(22) Eichkorn, K.; Weigend, F.; Treutler, O.; Ahlrichs, R. *Theor. Chem. Acc.* **1997**, *97*, 119.
(23) Frisch, M. J.; Trucks, G. W.; Schlegel, H. B.; Scuseria, G. E.; Robb, M. A.; Cheeseman, J. R.; Montgomery, J. A., Jr.; Vreven, T.; Kudin, K. N.; Burant, J. C.; Millam, J. M.; Iyengar, S. S.; Tomasi, J.; Barone, V.; Mennucci, B.; Cossi, M.; Scalmani, G.; Rega, N.; Petersson, G. A.; Nakatsuji, H.; Hada, M.; Ehara, M.; Toyota, K.; Fukuda, R.; Hasegawa, J.; Ishida, M.; Nakajima, T.; Honda, Y.; Kitao, O.; Nakai, H.; Klene, M.; Li, X.; Knox, J. E.; Hratchian, H. P.; Cross, J. B.; Adamo, C.; Jaramillo, J.; Gomperts, R.; Stratmann, R. E.; Yazyev, O.; Austin, A. J.; Cammi, R.; Pomelli, C.; Ochterski, J. W.; Ayala, P. Y.; Morokuma, K.; Voth, G. A.; Salvador, P.; Dannenberg, J. J.; Zakrzewski, V. G.; Dapprich, S.; Daniels, A. D.; Strain, M. C.; Farkas, O.; Malick, D. K.; Rabuck, A. D.; Raghavachari, K.; Foresman, J. B.; Ortiz, J. V.; Cui, Q.; Baboul, A. G.; Clifford, S.; Cioslowski, J.; Stefanov, B. B.; Liu, G.; Liashenko, A.; Piskorz, P.; Komaromi, I.; Martin, R. L.; Fox, D. J.; Keith, T.; Al-Laham, M. A.; Peng, C. Y.; Nanayakkara, A.; Challacombe, M.; Gill, P. M. W.; Johnson, B.; Chen, W.; Wong, M. W.; Gonzalez, C.; Pople, J. A. *Gaussian 03*, revision C.02; Gaussian, Inc.: Wallingford, CT, 2004.
(24) Dierksen, M.; Grimme, S. *J. Chem. Phys.* **2004**, *120*, 3544–3554.
(25) Santoro, F.; Lami, A.; Improta, R.; Bloino, J.; Barone, V. *J. Chem. Phys.* **2008**, *128*, 22431.
(26) Ahlrichs, R.; Bar, M.; Hasel, M.; Horn, H.; Komel, C. *Chem. Phys. Lett.* **1989**, *162*, 165.
(27) TURBOMOLE; see http://www.turbomole.de/.
(28) Negri, F.; Orlandi, G. In *Computational Photochemistry*; Olivucci, M., Ed.; Elsevier: New York, 2005; Vol. 16, pp 129−169.
(29) Mohanty, Y.; Nau, W. M. *Photochem. Photobiol. Sci.* **2004**, 1026–1031.
(30) Strickler, S. J.; Berg, R. A. *J. Chem. Phys.* **1962**, *37*, 814–822.
(31) Jankowiak, H. C.; Stuber, J. L.; Berger, R. *J. Chem. Phys.* **2007**, *127*, 234101.
(32) Santoro, F.; Improta, R.; Lami, A.; Bloino, J.; Barone, V. *J. Chem. Phys.* **2007**, *126*, 084509.
(33) Santoro, F.; Lami, A.; Improta, R.; Barone, V. *J. Chem. Phys.* **2007**, *126*, 184102.
(34) Dierksen, M.; Grimme, S. *J. Chem. Phys.* **2005**, *122*, 244101.
(35) Borrelli, R.; Peluso, A. *J. Chem. Phys.* **2003**, *119*, 8437–8448.
(36) Duschinsky, F. *Acta Physicochim. URSS* **1937**, *7*, 551.
(37) Zgierski, M. *Z. Chem. Phys.* **1986**, *108*, 61–68.
(38) Barone, V.; Bloino, J.; Biczysko, M.; Santoro, F. *J. Chem. Theory Comput.* **2009**, *5*, 540–554.
(39) Grimme, S. *Reviews in Computational Chemistry*; Wiley-VCH: New York, 2004; Vol. 20, pp 153−218.
(40) Bandyopadhyay, I. *Bull. Korean Chem. Soc.* **2003**, *24*, 717–722.
(41) Montalti, M.; Credi, A.; Prodi, L.; Gandolfi, M. T. *Handbook of Photochemistry*, 3rd ed.; CRC Press: Boca Raton, FL, 2006.
(42) Wallace, W. L.; Van Duyne, R. P.; Lewis, F. D. *J. Am. Chem. Soc.* **1976**, *98*, 5319–5326.
(43) Schmidt-Mende, L.; Fechtenkotter, A.; Mullen, K.; Moons, E.; Friend, R. H.; MacKenzie, J. D. *Science* **2001**, *293*, 1119–1122.

JP9005247